JOURNAL OF Applied Polymer SCIENCE

# Enhanced Mechanical and Thermal Properties of Biodegradable Poly(butylene succinate-*co*-adipate)/Graphene Oxide Nanocomposites via *In Situ* Polymerization

**Weidong Zhou, Xiaowei Wang, Pingli Wang, Wei Zhang, Junhui Ji**
Technical Institute of Physics and Chemistry, Chinese Academy of Science, Beijing, China, 100190
Correspondence to: J. Ji (E-mail: jijunhuichina@gmail.com)

**ABSTRACT:** Poly(butylene succinate-*co*-butylene adipate) (PBSA)/graphene oxide (GO) nanocomposites were synthesized via *in situ* polymerization for the first time. Atomic force microscopy demonstrated the achievement of a single layer of GO, and transmission electron microscopy proved the homogeneous distribution of GO in the PBSA matrix. Fourier transform infrared spectroscopy results showed the successful grafting of PBSA chains onto GO. With the incorporation of 1 wt % GO, the tensile strength and flexural modulus of the PBSA were enhanced by 50 and 27%, respectively. The thermal properties characterized by differential scanning calorimetry and thermogravimetric analysis showed increases in the melting temperatures, crystallization temperatures, and thermal stability.


**KEYWORDS:** biodegradable; composites; mechanical properties; thermal properties

Received 14 January 2013; accepted 6 May 2013; Published online 8 July 2013
**DOI: 10.1002/app.39512**

## INTRODUCTION

In recent years, biodegradable plastics have attracted great attention because the environmental problems caused by plastics have become more and more serious. Poly(butylene succinate-*co*-butylene adipate) (PBSA; with 20 mol % butylene adipate), with the trademark BIONOLLE, is a random copolyester of 1,4-butanediol, succinic acid, and adipic acid, has a greater impact strength and is more susceptible to biodegradation than other commercial biodegradable plastics, such as poly(lactic acid) (PLA) and poly(butylene succinate) (PBS).[1–3]

However, the flexible chains of PBSA result in the deficiency of other performances; for example, it has a low hardness, slow crystallization rate, and low thermal stability, the values of which are often not sufficient for a wide range of end-use applications.[4,5] Therefore, methods for improving its intrinsic properties to achieve more requirements have attracted much technological and commercial interest. Among these methods, the introduction of inorganic nanofillers, such as montmorillonite, organoclay, and carbon nanotubes, has been shown to have a remarkable influence on the performance of the nanocomposites.[6–10]

As nanofillers, graphene nanosheets (GNSs) and graphene oxide (GO) have drawn tremendous attention over the years. Compared to the virgin biodegradable polymers, GNS- and GO-based nanocomposites have significantly improved mechanical performance and thermal stability.[11–13] Wang et al.[14] increased the tensile strength of PBS by 21% and the storage modulus by 24% at a 2 wt % GNS loading, and the thermal stability of the nanocomposite was also enhanced. Increases of 51% in Young's modulus and 91% in the tensile strength of chitosan incorporating 1 wt % GO were achieved by Pan et al.[15] Cao et al.[16] raised the Young's modulus of PLA by 18% with the addition of only 0.2 wt % reduced GO. Pinto et al.[17] also showed improvements in the mechanical properties of PLA incorporated with very small loadings of GNSs or GO. Yoon et al.'s[18] results showed a two- to three-fold increase in the tensile modulus of poly(lactic-*co*-glycolic acid)/GO composite films compared to that of a poly(lactic-*co*-glycolic acid) film. Apart from the improved properties arising from the addition of GNSs or GO to biodegradable polymers, the corresponding nanocomposites retained biodegradability. One of the other advantages of GNS- or GO-based nanocomposite technology is that there is generally a significant improvement in the biocompatibility of the nanocomposites.[19,20] Some of the findings indicate that biodegradable nanocomposites embedded with GNSs or GO are attractive candidates for use in biomedical applications.

Compared to GNSs, GO can be easily prepared, and it can promote the dispersion of GNSs in the polymer matrix. Additionally, hydroxyl, epoxide, and carboxyl functional side groups on the surface of GO can improve the interfacial bonding between

the GO and the polymers. What is more, among the three main techniques used for the preparation of GO-based biodegradable nanocomposites, including solution-based processing, melt intercalation, and *in situ* polymerization, the last technique is attractive because it can guarantee both the dispersion and the interfacial bonding. Hence, in this study, we synthesized nanocomposites of PBSA and GO via *in situ* polymerization. Such nanocomposites have achieved a nanoscale homogeneous dispersion of GO and strong interfacial interaction between GO and PBSA matrix, nd we further characterized the morphology, molecular weight, and mechanical and thermal properties the nanocomposites.

## EXPERIMENTAL

### Materials

Graphite powder, with an average particle size of 1 mm and a purity greater than 99%, was purchased from Alfa Aesar. Succinic acid (≥99%), adipic acid (≥99%), 1,4-butanediol (99%), and titanium butoxide (≥98%) were obtained from Aladdin Reagent Co., Ltd. (Shanghai, China). Nitric acid ($HNO_3$, 65%), sulfuric acid ($H_2SO_4$, 98%), potassium permanganate ($KMnO_4$), hydrogen peroxide ($H_2O_2$, 30%), and other chemical reagents were purchased from Sinopharm Chemical Reagent Beijing Co. (Beijing, China). All materials were used without further purification.

### Preparation of GO and Poly(butylene succinate-*co*-butylene adipate)/Graphene Oxide (PG) Nanocomposites

Graphite oxide was prepared from graphite powder according to the method described by Hummers and Richard.[21] First, 5 g of graphite powder was put into a 500-mL flask containing 33 mL of $HNO_3$ and 200 mL of $H_2SO_4$. Then it was stirred for 30 min in an ice bath, and we added 30 g of $KMnO_4$. The solution temperature was raised gradually to 40°C and maintained there for 30 min. After that, the excess $KMnO_4$ was removed by treatment with $H_2O_2$ and washed several times with distilled water until a pH of 6 or greater was reached. Last, the graphite oxide was obtained by centrifugation at 10,000 rpm for 20 min and dried *in vacuo* at 50°C for 3 days.

A typical procedure for preparing PG nanocomposites with a 0.2 wt % GO content is depicted as follows: 0.2 g of graphite oxide, 50 mL of water, and 54 g (0.6 mol) of 1,4-butanediol were loaded into a 500-mL, four-necked, round-bottom flask, and the mixture was sonicated at 60°C for 2 h to obtain a homogeneous solution of GO; this was followed by the addition of 47.2 g (0.4 mol) of succinic acid, 14.6 g (0.1 mol) of adipic acid, and 0.034 g (0.0001 mol) of titanium butoxide. After the flask was equipped with a mechanical stirrer and an $N_2$ inlet, the mixture was heated to 180°C and maintained there for 3 h. Then polycondensation was done at 220°C under a reduced pressure of 10 Torr for 4 h. Finally, the polymerization led to the *in situ* formation of the PBSA matrix, which was accompanied by the nanoscale exfoliation of GO and its gradual dispersion. Before the final products were cooled down in the flask, they were directly pulled out and stored in a vacuum oven. According to their weight percentage of GO, the PG nanocomposites were labeled PG-0.2, PG-0.5, and PG-1, respectively. Pure PBSA without GO was prepared with the same procedures and used as a control.

To investigate the interactions between PBSA and the GO surface, successive centrifugation/redissolution cycles were used to separate the GO from the physically absorbed PBSA.[22,23] Briefly, we dispersed a portion of PG-1 in chloroform, and the solution was centrifuged at 10,000 rpm for 30 min. The operation was performed five more times to ensure that the physically absorbed free polymers were completely removed. Then, the PBSA grafted on GO was dried in a vacuum oven at 80°C for 24 h. The isolated filler from the polymer matrix was labeled P-*g*-G.

### Measurements

The weight-average molecular weight ($M_w$) was determined by gel permeation chromatography. Each sample was dissolved in chloroform, and the solution was filtered with a 0.2-$\mu$m Teflon filter before measurement. For atomic force microscopy (AFM), the aqueous GO suspension was spin-coated onto freshly cleaved mica surfaces. For transmission electron microscopy (TEM), sliced thin sections of the PG nanocomposites with a thickness of about 50–70 nm, prepared by ultramicrotomy, were used to take the TEM images of the nanocomposites. X-ray diffraction (XRD) patterns were recorded on a Bruker D8 focus. The scans ranged from 5 to 60° with a scanning rate of 6°/min. Fourier transform infrared (FTIR) spectra were collected in the region 4000–600 $cm^{-1}$ with a spectral resolution of 4 $cm^{-1}$ and 32 scans co-added. Test specimens for the tensile and flexural measurements were done with an Instron tester. The dumbbell-shaped samples (25 × 4 × 2 $mm^3$) were stretched at 25°C at a 50 mm/min stretching rate. The samples for flexural modulus were 80 × 10 × 2 $mm^3$ in dimension with a crosshead speed of 0.4 mm/min. The thermal transitions were measured with a Setaram differential scanning calorimetry (DSC) instrument. About 6 mg of each sample was heated from room temperature to 150°C at a rate of 10°C/min and kept there for 5 min to erase any thermal history. Then, the sample was cooled to −50°C at 10°C/min, maintained there for 5 min, and heated again to 150°C at the same rate. The decomposition characteristics of the samples were determined with a Pyris1 thermogravimetric analysis (TGA) instrument. About 5 mg of each sample was placed in the pan and heated from 25 to 600°C at a rate of 10°C/min under a nitrogen atmosphere.

## RESULTS AND DISCUSSION

### Morphology

To illustrate the complete exfoliation of GO and its characteristics, AFM was used in this work. Figure 1(a) shows the GO synthesized by the previous method. We can see that the GO sheets were about 1 nm thick; this suggested a full exfoliation of GO by the ultrasonic treatment. To further reveal the dispersion state of GO in the PBSA matrix, TEM was used to observe the section of PG-1. As shown in Figure 1(b), the GO layers were homogeneously distributed in the PBSA matrix polymer to form continuous networks. In combination with the AFM and TEM images, this confirmed that the GO nanosheets were exfoliated well into single layers and homogeneously dispersed in the matrix.

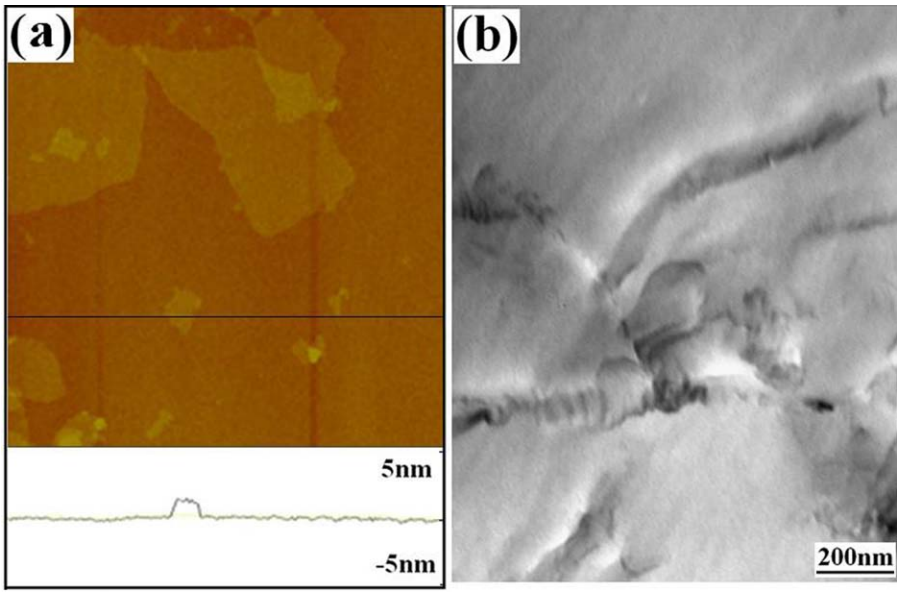


**Figure 1.** (a) AFM of GO and (b) TEM image of the PG-1 nanocomposites. [Color figure can be viewed in the online issue, which is available at wileyonlinelibrary.com.]

### Molecular Weight

The molecular weight of PBSA and the nanocomposites are shown in Table I. The presence of GO during the polymerization of PBSA influenced the growth of chains so that $M_w$ decreased from 62,400 g/mol for neat PBSA to 45,500 g/mol for PG-1. The excessive carboxylic acid and hydroxyl groups on GO probably inevitably disrupted the stoichiometric balance in the reaction system and simultaneously terminated the potential propagation of active chains ends. On the other hand, the GO might have represented a physical obstruction for the organization of the polymer segments during the polymerization.

### Chemical and Crystal Structure

To certify the reaction between the end groups of PBSA and the groups on GO, we measured the infrared spectra of the GO, P-*g*-G, PBSA, and PG-1. As shown in Figure 2, for the GO sample, the characteristic vibrations included the O—H stretching vibrations at 3430 $cm^{-1}$, the weak C═O peak in carboxylic acid and carbonyl moieties at 1725 $cm^{-1}$, C—OH peak at 1380 $cm^{-1}$, C—O—C peak at 1240 $cm^{-1}$, and C—O stretching peak at 1065 $cm^{-1}$. The differences between the spectra of P-*g*-G and GO were obvious at the peaks of 1725, 1653, and 1152 $cm^{-1}$, which were the characteristic absorption bands of C═O, C═C, and C—O, respectively. So, we concluded that GO was successfully grafted by the PBSA chains because the peaks of C═O and C—O on P-*g*-G were obviously strengthened. In addition, Figure 2 shows the negligible effect of the GO on the spectra of the PBSA; this indicated that it was difficult to directly identify the formation of ester bonds between the PBSA and GO because the PBSA backbones had the same ester bonds. However, it was clear that the band at 3430 $cm^{-1}$ for O—H groups in the GO decreased in the spectra of P-*g*-G, and it disappeared in the spectra of PG. In summary, these results verify that some PBSA chains were successfully grafted on the GO sheets during *in situ* polymerization. The functional groups of —OH and —COOH could have provided active sites to form chemical bonds and acted as an ideal interface between the GO and PBSA, which could form ester bonds by reaction between the end of the PBSA

**Table I.** Molecular Weights of the PBSA and PG Nanocomposites

| Sample | $M_n$ | $M_w$ | PDI |
|---|---|---|---|
| PBSA | 36,100 | 62,400 | 1.7 |
| PG-0.2 | 31,700 | 59,800 | 1.9 |
| PG-0.5 | 28,300 | 47,300 | 1.7 |
| PG-1 | 26,900 | 45,500 | 1.7 |

$M_n$, number-average molecular weight; PDI, polydispersity index.

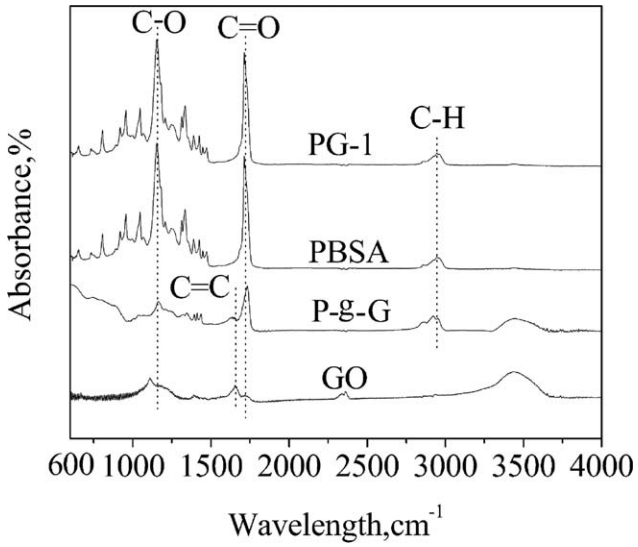


**Figure 2.** FTIR spectra of the GO, P-*g*-G, neat PBSA, and PG-1 nanocomposites.

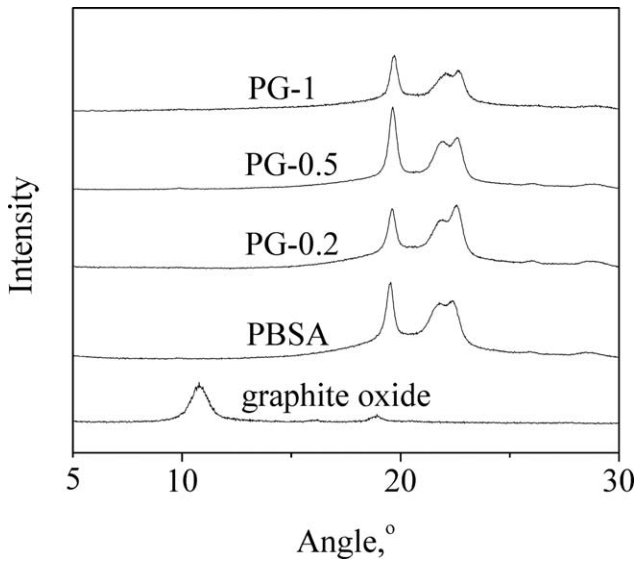


**Figure 3.** XRD patterns of the graphite oxide, neat PBSA, and PG nanocomposites.

chains and groups on the GO. Similar grafting reactions between polyesters and GO have been also demonstrated for other nanocomposites, including PLA and PBS.[19,24–26]

XRD was an important tool for determining whether graphite oxide is exfoliated to individual GO sheets in the nanocomposites; we used it to study the influence of GO on the crystal structure of the polymer in the nanocomposites. Figure 3 shows the XRD patterns of graphite oxide, neat PBSA, and the PG nanocomposites. First, the reflection of graphite oxide was present around a $2\theta$ value of 10.8°, whereas it was absent in the PG nanocomposites; this suggested that the layered graphite oxide was exfoliated in the nanocomposites without obvious stacking. Although this did not necessarily mean that all of the stacking was lost, it did indicate the disordered stacking structure of the GO. Then, PBSA showed three strong diffraction peaks located at $2\theta$ values of 19.5, 21.8, and 22.4°. The three diffraction peaks from small to high angles were assignable to the (020), (021) and (110) planes, respectively. The XRD patterns of the PG nanocomposites had three similar strong diffraction peaks to PBSA; this indicated that the incorporation of GO did not modify the crystal structure of PBSA in the nanocomposites.

### Mechanical Properties

Figure 4(a) shows the stress ($\sigma$)–strain ($\varepsilon$) curves of the PBSA and the PG nanocomposites with different GO contents. All of them showed the typical $\sigma$–$\varepsilon$ curve for a conventional polymer with yielding. The tensile strengths of the PG nanocomposites were gradually enhanced with the addition of GO. However, the elongation at break decreased with increasing GO content. As shown in Figure 4(b), the flexural modulus of each of the PG nanocomposites was significantly enhanced. Compared to those of the neat PBSA, the tensile strength and flexural modulus of PG-1 were increased by 50% from 28 to 42 MPa and by 27% from 434 to 551 MPa, respectively. We concluded that the high degree of dispersion of the intercalated GO layers inside the PBSA matrix by *in situ* polymerization was the key responsible factor for the remarkable increase in the mechanical properties. Undoubtedly, the excellent reinforcement of GO could also have been attributed to the strong interaction between the GO and PBSA matrix. On the other hand, the reactions between PBSA and GO reduced the flexibility of the molecular chains and inhibited their activities; this led to increases in the tensile strength and flexural modulus and decreases in the elongation at break. These results were consistent with the studies of other researchers.[27]

### Thermal Properties

DSC experiments on pure PBSA and the nanocomposites were carried out to understand the effect of GO incorporation on the thermal properties of PBSA. According to Figure 5(a), the melting curves of PG were similar to those of neat PBSA, but the melting temperature ($T_m$) of each of the nanocomposites tended to increase roughly, from 92.3°C in neat PBSA to 95.0°C in

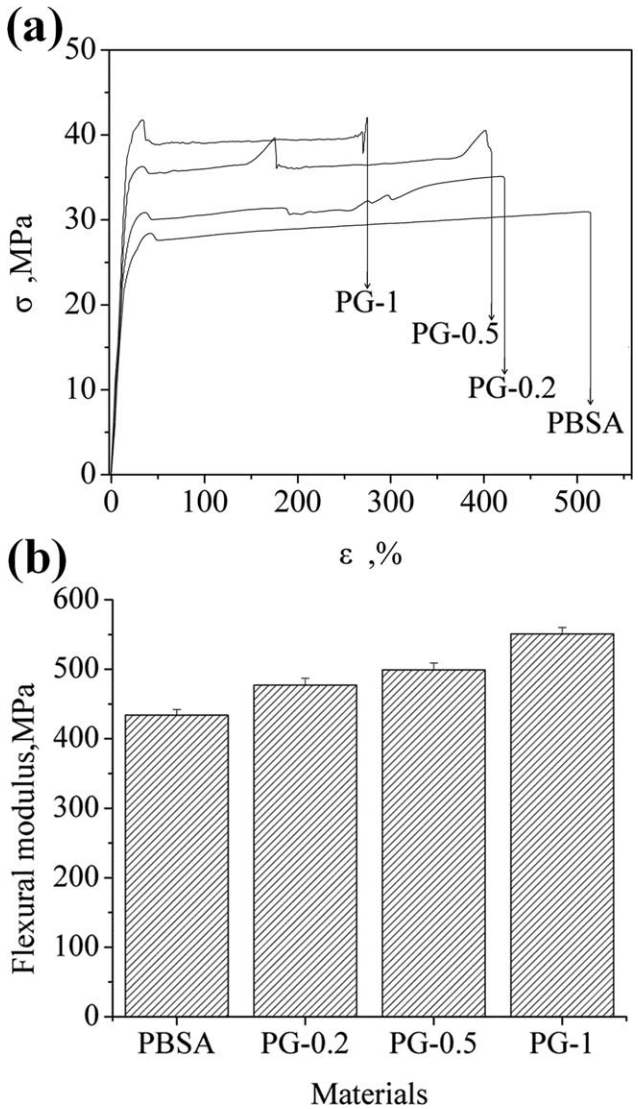


**Figure 4.** (a) $\sigma$–$\varepsilon$ curves and (b) flexural modulus of the neat PBSA and PG nanocomposites.

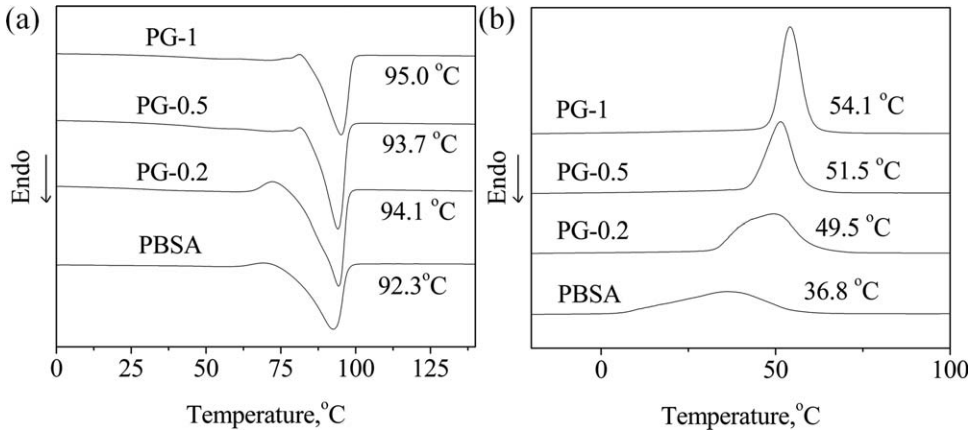


**Figure 5.** (a) Melt behaviors and (b) melt crystallization behaviors of the PBSA and PG nanocomposites.

PG-1. We suggest that the strong bonding interactions between GO and PBSA affected the mobility of the PBSA polymer chains, which led to the increase in $T_m$.

Figure 5(b) illustrates the DSC cooling traces for neat PBSA and its three nanocomposites during the melt crystallization. As shown, the crystallization temperature ($T_c$) of neat PBSA was 36.8°C; however, the value shifted up to 49.5, 51.5, and 54.1°C in PG-0.2, PG-0.5 and PG-1, respectively. We confirmed that the presence of GO greatly enhanced the melt crystallization of PBSA in the nanocomposites. In our opinion, depending on their size and distribution, both GO and P-*g*-G acted as nucleating agents and strongly affected the crystallization kinetics of the PBSA matrix; this contributed favorably to the faster rate of crystallization. Similar results have also been found recently in PBS/GO nanocomposites and PLA/GO nanocomposites.

In addition, the thermal stability of these materials was also mildly improved. Figure 6 shows typical TGA traces of weight loss as a function of temperature for the pure PBSA and PG nanocomposites. It was clear that PG nanocomposites exhibited a higher thermal stability compared to the neat PBSA, where the peak decomposition temperatures were 378.8, 382.4, 387.2, and 387.7°C for pure PBSA, PG-0.2, PG-0.5, and PG-1, respectively. The amount of GO played an important role in the thermal stabilization of PBSA; the GO stabilized the decomposition of PBSA, which corresponded well with recent reports.[28] This could have been the reason that the GO acted as a superior insulator and mass transport barrier to the volatile products generated during decomposition, and the creation of a tortuous path, resulting from the dispersion of GO in the PBSA matrix, slowed the diffusion of the produced substances in the material.

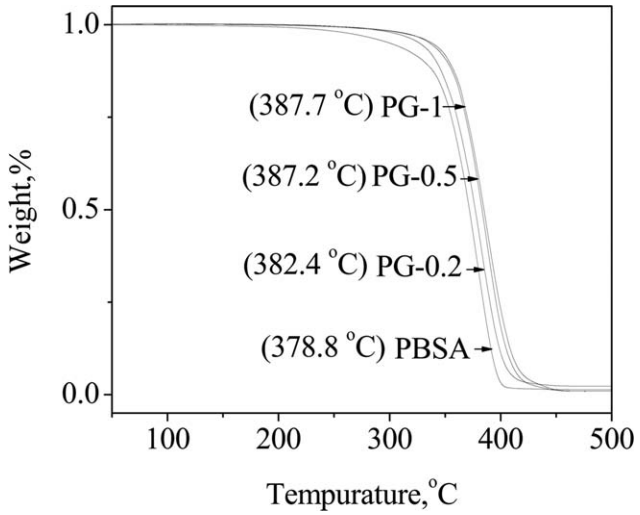


**Figure 6.** TGA traces of the PBSA and PG nanocomposites.

## CONCLUSIONS

In this study, we successfully synthesized PG nanocomposites with well-dispersed GO sheets by *in situ* polymerization. The GO was prepared well by the ultrasonic treatment of graphite oxide. The mechanical properties of the nanocomposites were greatly elevated as a result of the single layer of GO, the homogeneous distribution, and the grafting structure of the PBSA chains onto GO. Specifically, the tensile strength and flexural modulus of the PG-1 were enhanced by 50 and 27%, respectively. Moreover, improvements in the thermal properties, including $T_m$, $T_c$, and the thermal stability, were also achieved. In the future, GO-based nanocomposites will have more potential applications as biodegradable materials because of these improved properties.

## ACKNOWLEDGMENTS

The authors thank the National Natural Science Foundation of China (contract grant numbers 51003114 and 51103170) and the National High Technology Research and Development Program of China (863; contract grant number 2011AA02A203).

## REFERENCES

1. Fujimak, T. *Polym. Degrad. Stab.* **1998**, *59*, 209.
2. Nikolic, M. S.; Djonlagic, J. *Polym. Degrad. Stab.* **2001**, *74*, 263.
3. Tserki, V.; Matzinos, P.; Pavlidou, E.; Vachliotis, D.; Panayiotou, C. *Polym. Degrad. Stab.* **2006**, *91*, 367.

4. Yang, F.; Qiu, Z.; Yang, W. *Polymer* **2009**, *50*, 2328.
5. Ojijo, V.; Malwela, T.; Ray, S. S.; Sadiku, R. *Polymer* **2012**, *53*, 505.
6. Ray, S. S.; Bousmina, M.; Okamoto, K. *Macromol. Mater. Eng.* **2005**, *290*, 759.
7. Chen, G.; Yoon, J. S. *Polym. Int.* **2005**, *54*, 939.
8. Kim, H. S.; Park, B. H.; Yoon, J. S.; Jin, H. *J. Polym. Int.* **2007**, *56*, 1035.
9. Tsimpliaraki, A.; Zuburtikudis, I.; Marras, S. I.; Panayiotou, C. *Polym. Int.* **2011**, *60*, 859.
10. Zhu, S.; Zhao, Y.; Qiu, Z. *J. Appl. Polym. Sci.* **2012**, *124*, 4268.
11. Ma, J.; Liu, C.; Li, R.; Wang, J. *J. Appl. Polym. Sci.* **2012**, *123*, 2933.
12. Zhang, J.; Qiu, Z. *Ind. Eng. Chem. Res.* **2011**, *50*, 13885.
13. Jing, X.; Qiu, Z. *Ind. Eng. Chem. Res.* **2012**, *51*, 13686.
14. Wang, X.; Yang, H.; Song, L.; Hu, Y.; Xing, W.; Lu, H. *Compos. Sci. Technol.* **2011**, *72*, 1.
15. Pan, Y.; Bao, H.; Li, L. *Am. Chem. Soc. Appl. Mater. Interfaces* **2011**, *3*, 4819.
16. Cao, Y.; Feng, J.; Wu, P. *Carbon* **2010**, *48*, 3834.
17. Pinto, A. M.; Cabral, J.; Tanaka, P.; Mendes, M. A.; Magalhaes, F. D. *Polym. Int.* **2013**, *62*, 33.
18. Yoon, O. J.; Sohn, Y.; Kim, D. J.; Lee, N. E. *Macromol. Res.* **2012**, *20*, 789.
19. Yoon, O. J.; Jung, C. Y.; Sohn, Y.; Kim, H. J.; Hong, B.; Jhon, M. S.; Lee, N. E. *Compos. A* **2011**, *42*, 1978.
20. Pinto, A. M.; Moreira, S.; Goncalves, I. C.; Gama, F. M.; Mendes, A. M.; Magalhaes, F. D. Colloids Surf. B, to appear.
21. Hummers, W. S.; Richard, E. O. *J. Am. Chem. Soc.* **1985**, *80*, 1339.
22. Liu, K.; Chen, L.; Chen, Y.; Wu, J.; Zhang, W.; Chen, F. *Mater. Chem.* **2011**, *21*, 8612.
23. Zhou, W.; Xu, T.; Wang, X.; Zhi, E.; Liu, L.; Zhang, W.; Ji, J. *J. Appl. Polym. Sci.* **2013**, *127*, 733.
24. Wang, X.; Zhang, C.; Liu, X.; Wang, P.; Zhang, W.; Zhao, J.; Ji, J. *Langmuir* **2012**, *28*, 7091.
25. Tang, Z.; Kang, H.; Shen, Z.; Guo, B.; Zhang, L.; Jia, D. *Macromolecules* **2012**, *45*, 3444.
26. Xu, Z.; Gao, C. *Macromolecules* **2010**, *43*, 6716.
27. Liang, J.; Huang, Y.; Zhang, L.; Wang, Y.; Ma, Y.; Guo, T.; Chen, Y. *Adv. Funct. Mater.* **2009**, *19*, 2297.
28. Yang, J. H.; Lin, S. H.; Lee, Y. D. *Mater. Chem.* **2012**, *22*, 10805.